15ÈMES JOURNÉES DE L'HYDRODYNAMIQUE
22 - 24 novembre 2016 - Brest

MODÉLISATION NON-LINÉAIRE DU GALOP EN ROTATION POUR DES CYLINDRES CARRÉS, RECTANGULAIRES

NON LINEAR MODEL OF ROTATIONAL GALLOPING OF SQUARE, RECTANGULAR AND BUNDLE CYLINDER IN CROSS-FLOW

Jacques Garapin [(1)], **Cédric Béguin** [(1)], **Stéphane Étienne*** [(1)]
Dominique Pelletier [(1)], **Bernard Molin** [(2)]
[(1)] Ecole Polytechnique de Montréal, [(2)] Ecole Centrale de Marseille

Résumé

L'apparition du galop en torsion est étudiée au moyen de simulations numériques bidimensionnelles, avec un code éléments finis conçu spécialement pour les problèmes couplés d'interactions fluide-structure. La comparaison entre simulations statiques en écoulement transversal et simulations dynamiques en mouvement d'oscillations forcées permet de mesurer l'amortissement fluide. Deux façons de modéliser cet amortissement sont développées. On confronte nos résultats à des expériences numériques en mouvement libre, en utilisant le cycle limite d'oscillation et la vitesse réduite comme critères de comparaison, lorsqu'on peut les mesurer. On montre que le modèle quasi statique n'est pas valide sur des géométries élancées, même si la mesure de l'amortissement sans introduire d'effets d'histoire permet de prédire précisément les plages d'instabilités.

Summary

The occurrence of rotational galloping for several geometries is assessed through two-dimensional flow simulations and fluid-structure interaction simulations. A finite element formulation specifically devised for fluid-structure interactions simulations has been used. Non-linear models aimed at predicting rotational galloping are determined based on cross-flow simulations around fixed cylinders for various angles of attack. The added torsional fluid damping coefficient is modelled based on the results of forced rotational oscillation simulations. The reliability of the models is assessed by confrontation with the results of free rotation simulations, where reduced velocity and maximum amplitude of galloping have been chosen as comparison criteria, when they can be measured. The quasi-steady model is shown to have strong limitations on streamlined bodies, even if a non-linear model with no history effect can precisely predict unstable zones.

*Address all correspondence to stephane.etienne@polymtl.ca

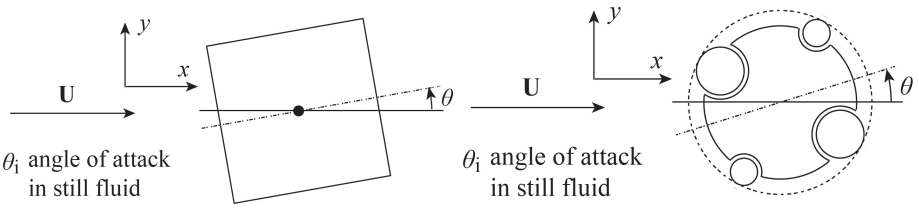

Figure 1: Arrangement of the mechanical system: notations, shape and sign convention.

1 Introduction

Rotational galloping can occur when a non-circular cylinder in cross-flow restrained by structural torsional stiffness can rotate around its axis. For some angles of attack, the variation of the moment acts as negative fluid stiffness or damping which leads to rotational vibrations. Comparatively to its transverse counterpart, the "rotational galloping is much more difficult to analyze" [5]. Robertson et al. (2003) compared rotational galloping quasi-steady predictions from Blevins quasi-steady model [2] with data obtained from fluid-structure interactions unsteady simulations [6]. Their results show that the quasi-steady criterion performs well at predicting the threshold of rotational galloping of rectangular cross sections. It remains however that, while very inexpensive, and thus appealing, the quasi-steady criterion validity is questionable due to the nature of the forces involved in torsional galloping.

A model starts with a way to write the added damping: we compare Blevins quasi-steady model (section 2, Eqn. 11), to an extension of this quasi-steady model (section 4, Eqn. 15) and to a Taylor 2^{nd} order expansion in position and velocity (section 5, Eqn. 18). To assess more accurately its possible validity, the criterion should be tested and confronted with results obtained on a variety of other section shapes. In this paper we consider a bundle cylinder section in addition to square section (shown in Fig. 1) and rectangular sections. The flow-induced stiffness, damping and inertia are determined from forced rotation oscillations results. All computations are performed with a finite element method. The solver has been specifically designed and developed to treat fluid-structure interactions with rigid or elastic structures.

2 Quasi-steady model

The occurrence and amplitude of transverse galloping are very well approached with a quasi-steady approach (see e.g.[3]). Transposing the theory to rotational galloping led to an *ad hoc* model based on moment coefficient derivative with respect to the angle of attack [2].

The averaged moment values are shown on Fig. 2 for the square and bundle sections at a Reynolds number of 200, following notations in Fig. 1. As the square section is symmetric with respect to the flow direction at zero angle of attack (see Fig. 1), the moment coefficient is an odd function of the angle of attack θ. Values are compared with those of two other references for the same value of the Reynolds number. Values compare very well with those obtained by Robertson et al. (2003) [6]. We suspect that the three-dimensional simulations results of Yoon et al. (2008) have been obtained with a too low spatial resolution [7].

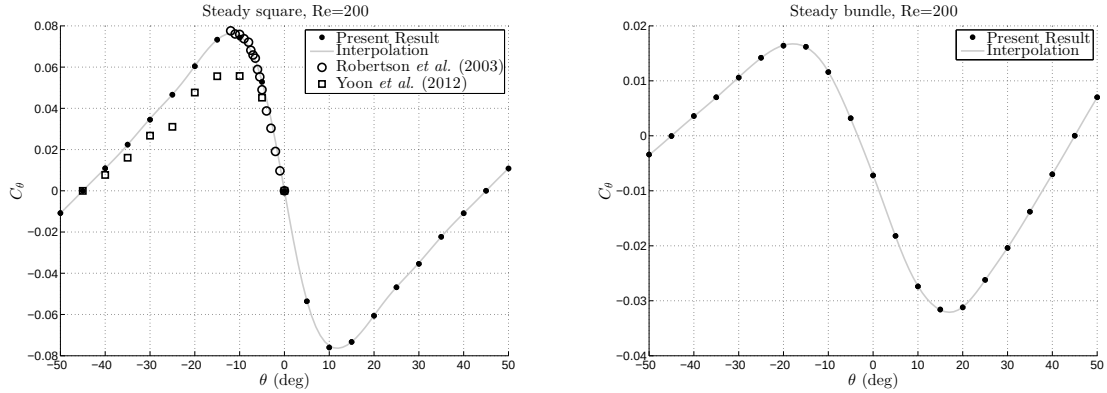

Figure 2: Coefficients of moment for a steady square and a steady bundle, C_θ and comparison with Robertson *et al.* (2003) and Yoon *et al.* (2012) [6], [7].

About the bundle, we see that there is no symmetry with respect to the midplane anymore. Note in passing that having chosen 45° or -45° as reference, the section would have been symmetric. However, the present choice makes it easier to compare with the square section. We observe a similar behaviour of the moment as function of the angle of attack compared to the square section, but not an odd function anymore due to the asymmetry of the bundle. The absolute maximum averaged moment is lower than for the square section. This might be due to two reasons. First recall that the outside diameter is equal to the square section edge. This makes the apparent bundle face smaller than that of the square. Also, the bundle section corners are rounded making the cylinder less sensitive to a change in angle of attack.

Removing the effect of von Karman's vortex street and history effect, the fluid moment around the structural central axis, M_θ, is assumed to be expressed as follows:

$$M_\theta(\theta,\dot{\theta},\ddot{\theta},Re) = \rho_f D^2 \left[\frac{U^2}{2} C_\theta(\theta) - UDC_{D\theta}(\theta,\dot{\theta},Re)\dot{\theta} - D^2 I_\theta(\theta,\dot{\theta},\ddot{\theta},Re)\ddot{\theta}\right] \tag{1}$$

The mechanical model of the free rotation of the section is:

$$I[\ddot{\theta} + 2\zeta\omega_n\dot{\theta} + \omega_n^2(\theta-\theta_i)] = M_\theta \tag{2}$$

Consequently, the angle of equilibrium θ_e is defined by:

$$I\omega_n^2(\theta_e-\theta_i) = M_\theta(\theta_e) \tag{3}$$

Including Eqn. (1) on the moment, the equation of motion becomes :

$$\left(1+\frac{I_\theta}{I^*}\right)\ddot{\theta} + 2\omega_n\left(\zeta + C_{D\theta}\frac{U_R}{4\pi I^*}\right)\dot{\theta} + \omega_n^2\left(1+\frac{U_R^2}{8\pi^2 I^*}K_\theta(\theta,\theta_e)\right)(\theta-\theta_e) = 0 \tag{4}$$

where

$$K_\theta(\theta,\theta_e) = -\frac{C_\theta(\theta)-C_\theta(\theta_e)}{\theta-\theta_e} \tag{5}$$

K_θ can be interpreted as a flow induced stiffness term. Static divergence can occur by negative stiffness if $K_\theta < 0$. Non linear terms will lead to a new equilibrium position.

$C_{D\theta}$ can be interpreted as a flow induced damping. Oscillations can occur by negative damping $C_{D\theta}(\theta_e) < 0$. Non linear terms will lead to a limit cycle.

C_θ and K_θ can be evaluated using steady case data. We obtain :

$$M_\theta(\theta = \theta_e, \dot{\theta} = 0, \ddot{\theta} = 0, Re) = \frac{\rho_f D^2 U^2}{2} C_\theta(\theta_e, Re) \tag{6}$$

and in first approximation according to Eqn. (5):

$$K_\theta(\theta_e) = -\frac{\partial C_\theta}{\partial \theta}(\theta_e) \tag{7}$$

Using the quasi steady theory, Blevins assumes that a rotating object sees an equivalent angle of attack [2]:

$$\alpha = \theta - \frac{L\dot{\theta}}{U} \tag{8}$$

with L a characteristic length, and that the equation for the moment can be simplified to:

$$\frac{M_\theta(\theta, \dot{\theta})}{\frac{1}{2}\rho_f U^2 D^2} = C_\theta(\alpha) \tag{9}$$

For small oscillations around θ_e in the quasi-steady regime where $U_R \gg 1$, we have $\dot{\theta} \ll \max(\theta - \theta_e)$ and $\theta_e - \theta \ll 1$ so that the Taylor expansion of $C_\theta(\alpha)$ is:

$$C_\theta(\alpha) = C_\theta(\theta_e) + \left(\theta - \theta_e - \frac{L\dot{\theta}}{U}\right) \frac{\partial C_\theta}{\partial \theta}(\theta_e) \tag{10}$$

Combining Blevins' assumption (Eqn. 9) with Eqn. (1) and (10) shows that $C_{D\theta}$ can be written as a constant:

$$C_{D\theta}(\theta_e, \dot{\theta}, Re) = \frac{L}{2D} \frac{\partial C_\theta}{\partial \theta}(\theta_e, Re) \tag{11}$$

The evaluation of the moment coefficient derivative involved in Eqn. (11) could easily be obtained from finite difference of time averaged moment histories at different values of the angle of attack. The criterion of possibility for torsional galloping becomes :

$$\frac{\partial C_\theta}{\partial \theta}(\theta_e) < 0 \tag{12}$$

3 Numerical simulations

In order to predict the critical reduced velocity of rotational galloping and the limit cycle, the effect of the rotational velocity and acceleration on fluid added damping and inertia must be determined. We proceed with numerical simulations of a forced motion to build a non-linear model, which will be implemented on free rotation simulations afterwards.

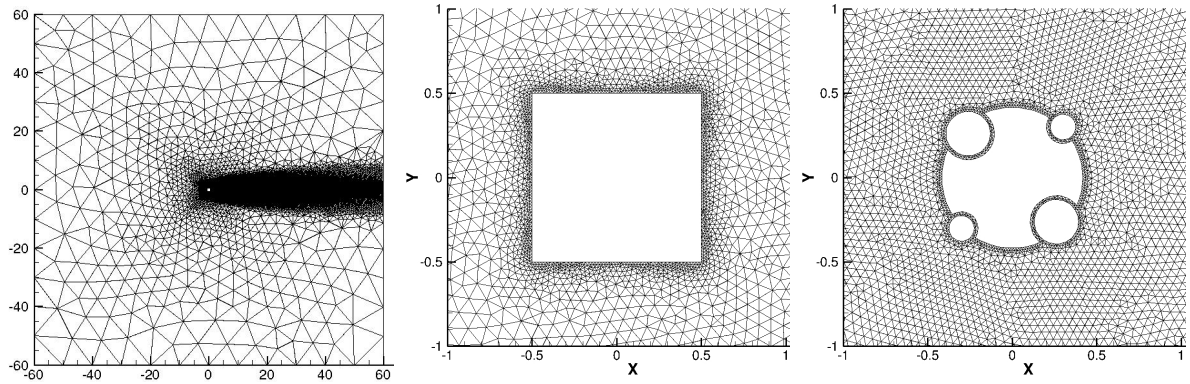

Figure 3: Views of the mesh: global view (left), proximity of the square cylinder (middle) and cylinder bundle (right).

Forced rotational oscillation

Simulations of forced rotational oscillations of both sections in cross-flow have been performed to determine the induced fluid flow damping and added inertia coefficients. The motion of both sections is:

$$\theta(t) - \theta_e = \Theta \sin\left(\frac{2\pi U}{U_R D} t\right) = \Theta \sin(\omega_n t) \tag{13}$$

For the calculations, we have set $Re = 200$ and $U_R = 40$. The simulations last until $t_f = 500$, which is enough to get an established regime and allows us to measure the moment on approximately 10 periods of the forced oscillations.

Numerical details

All computations are performed with a finite element method. The solver has been specifically designed and developed to treat fluid-structure interactions with rigid or elastic structures. The incompressible velocity-pressure formulation of the Navier-Stokes Equations is considered. 3^{rd} order space accuracy is achieved by using P2-P1 Taylor-Hood elements. In this study all simulations have been performed with an adaptive hp BDF method. We have set a tolerance error in time of order 10^{-5}. The solution strategy is direct implicit. All degrees of freedom are coupled. This code has been thoroughly verified and validated for unsteady flows on moving grids [4]. Details of the convergence study that was performed can be found in [1].

Figure 3 shows the mesh we employed for the simulations, and close-ups of the mesh where we can see the increased mesh density close to the walls to ensure appropriate flow resolution within the boundary layers. Note the refinement of the mesh in the wake area thanks to the unstructured mesh capabilities. Symmetry conditions are applied on top and bottom boundaries. Outlet conditions are ($u : \vec{\sigma}_x.\vec{n} = 0$, $v = 0$); inlet conditions are ($u = 1$,$v = 0$) for velocities in the x and y directions.

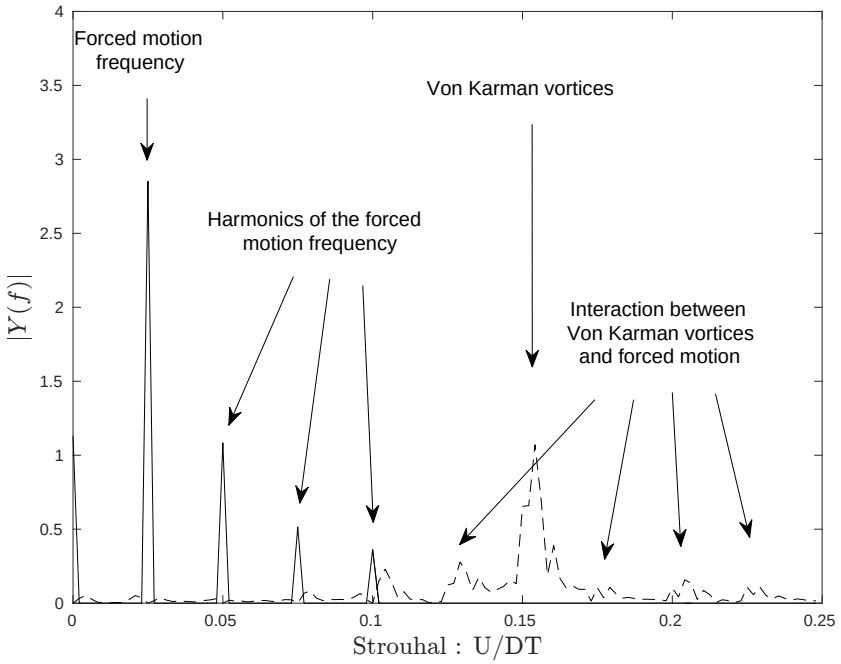

Figure 4: Spectrum of the moment, with the contribution of Von Karman vortices (dashed line), and the part of the moment responsible for galloping (solid line). Square section, $\theta_e = 5$, $\Theta = 20$.

4 Modelling with an extension of Blevins criterion

Post-processing

Data obtained from the computations is the moment exerted by the fluid on the solid against time, assuming there is no history effect. This moment is the sum of two contributions: the effect of Von Karman vortices in the wake of the cylinder, and the fluid moment in which we are interested. These two contributions can be seen on a Fourier transform of the signal (Fig. 4). The release frequency of Von Karman vortices is well documented: for the square, the associated Strouhal number is 0.15, as we can see in Fig. 4. Selecting the first 4 harmonics of the forced motion allows us to keep the relevant part of the signal. The fifth harmonics is too close from the vortex release frequency to be precisely measured.

Removing the effect of von Karman's vortex street thanks to this filter, we are able to plot the dimensionless torque responsible of galloping with respect to θ. We compare this moment with the measure in the steady cases, in Fig. 5(a) and 5(b). We observe that the steady case is a good approximation for the average value of the moment, even if dynamic effects appear for large amplitudes, especially when the slope of the static moment coefficient changes with the position. We can also notice that dynamic effects are more important on the square section.

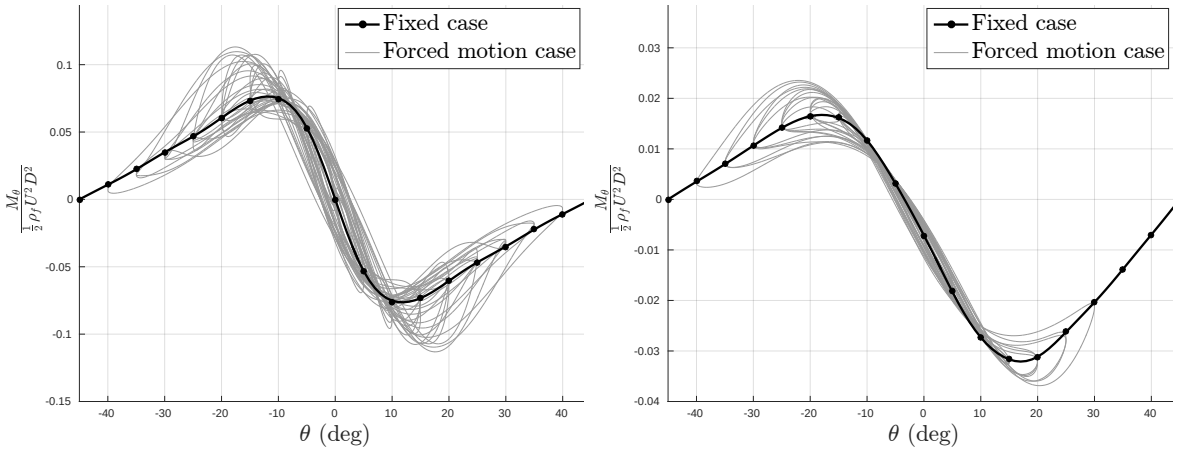

(a) Square section

(b) Bundle section

Figure 5: Torque against angular position during fixed motion (grey line) compared to fixed cases coefficient moment (bold black line), removing Von Karman effect.

Model for the added damping

According to Eqn. (1), measuring the moment when there is no angular acceleration gives information on $C_{D\theta}$:

$$\frac{M_\theta(\theta, \dot{\theta}, \ddot{\theta} = 0)}{\frac{1}{2}\rho_f U^2 D^2} = C_\theta(\theta) - \frac{2D}{U} C_{D\theta}(\theta, \dot{\theta})\dot{\theta} \tag{14}$$

As the movement is forced, Eqn. (14) shows that $C_{D\theta}$ can be evaluated for $\theta(t) = \theta_e$, $\dot{\theta}(t) = \pm\omega_n\Theta$. As stated in Eqn. (11), Blevins assumes that $C_{D\theta}$ can be expressed with the derivative of the static coefficient of moment C_θ with respect to θ. According to this assumption, we built the following model, where the effect of the velocity is developed to the second order:

$$C_{D\theta}(\theta, \dot{\theta}) = A + B\frac{\partial C_\theta}{\partial \theta}(\theta) + C\left(\frac{\dot{\theta}}{\omega_n}\right) + D\left(\frac{\dot{\theta}}{\omega_n}\right)^2 + E\left(\frac{(\theta - \theta_e)\dot{\theta}}{\omega_n}\right) \tag{15}$$

We measured $C_{D\theta}$ when $\theta = \theta_e$, what makes it impossible to evaluate E. It is assumed to be equal to zero. For the other coefficients, the best fit of the numerical values by the model is shown in Tab. 1. A and B are the most significant parameters of the model: B represents what Blevins denotes $L/2D$ in Eqn. (11). As L and D are set to 1, measuring $B \simeq 1/2$ seems to be consistent with this criterion. Parameter A can be related to the unavoidable damping induced by the friction. In case of a circular cylinder, $\frac{\partial C_\theta}{\partial \theta} = 0$ but a damping still exists, $A \neq 0$ and is certainly Reynolds dependent. The effect of the angular velocity on the damping seems to be negligible ($C = 0$, $D = 0$). From now on, the model is simplified, keeping the measured values for A and B, and setting C and D to zero for both geometries. Fitting the data with this simplified model does not modify the values for A and B. Comparison between the data and this simplified model is plot on Fig. 6.

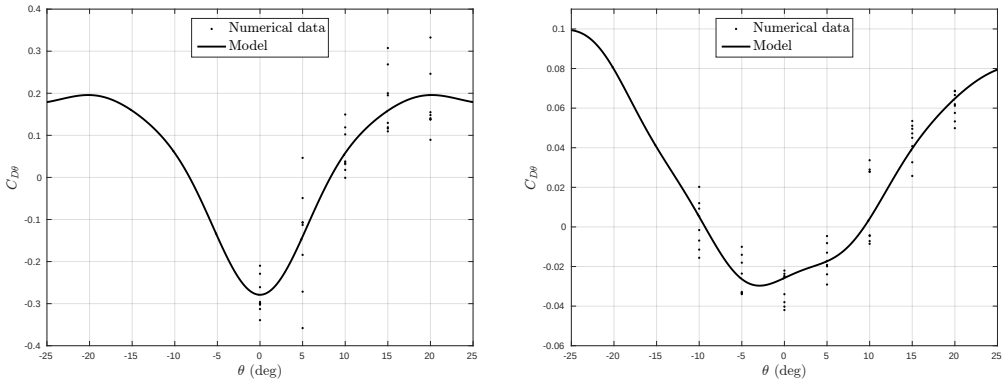

(a) Square section (b) Bundle section

Figure 6: Model for the added damping as a function of angle.

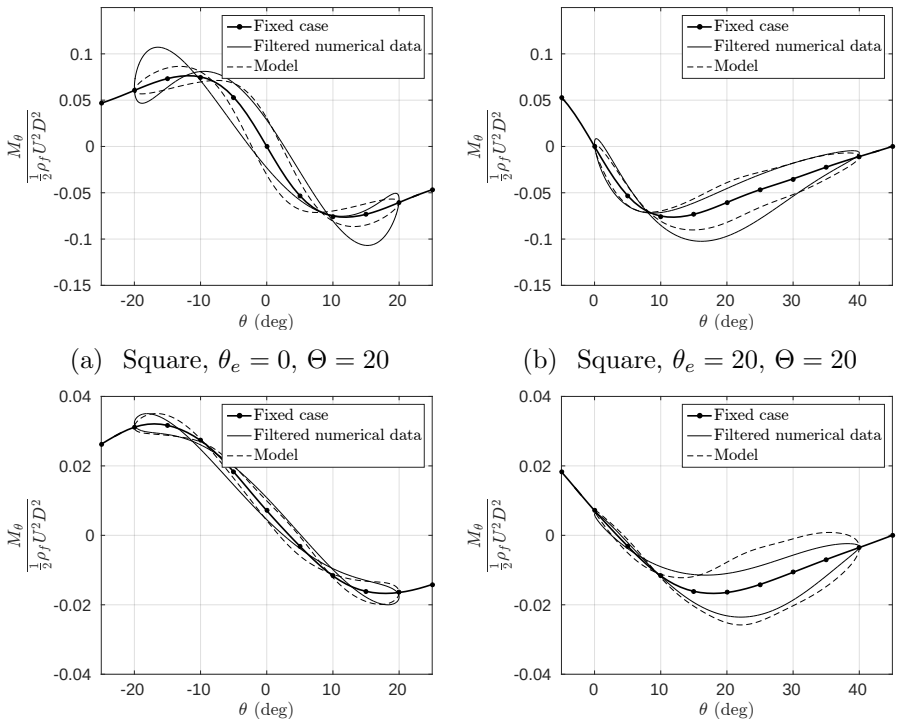

(a) Square, $\theta_e = 0$, $\Theta = 20$ (b) Square, $\theta_e = 20$, $\Theta = 20$

(c) Bundle, $\theta_e = 0$, $\Theta = 20$ (d) Bundle, $\theta_e = 20$, $\Theta = 20$

Figure 7: Comparison between the model and the filtered data, for the square (top) and the bundle (bottom) cylinders.

Table 1: Fitting coefficients.

Geometry	A	B	C	D
Square	0.08	0.49	0.00	0.00
Bundle	0.06	0.66	0.00	0.00

This model is built with the measures of the added damping when there is no acceleration. However, it is possible to compare our model to the numerical data, the gap between the model and the data being the effect of the added inertia. We calculate the expected moment from Eqn. (1), where $C_\theta(\theta)$ is known from the static case, $C_{D\theta}(\theta, \dot{\theta})$ is given by the model, with no added inertia ($I_\theta(\theta, \dot{\theta}, \ddot{\theta}) = 0$). Results are shown in Fig. 7 for both cylinders. The model seems to be a good approximation of the moment, even when angular acceleration is not equal to zero. We could deduce the value of added inertia from the difference between the two curves, but as the difference is small and acceleration is very low ($\mid \ddot{\theta} \mid \leq \omega_n^2 \Theta$, with $\omega_n \sim 10^{-1}$), we assume that added inertia is negligible compared to added stiffness and damping. An important feature of the model is its ability to predict the range over which the fluid gives energy to the solid. Between $\theta = 10°$ and $-10°$ approximately, damping is negative and the solid captures energy. The amplitude of the oscillation grows until the cylinder reaches a position at which the energy transfer goes from the solid to the fluid. We expect the equilibrium amplitude to be reached when the area enclosed by the curve corresponding to a positive damping ($|\theta| > 10°$) equals the area corresponding to a negative damping ($|\theta| < 10°$), on Fig. 7.

Free motion

To asses the reliability of our model, we consider the free rotations of sections around their central axis. Sections are restrained by torsional stiffness. Eqn. (16) is numerically solved with $U_R = 40$, $c_s = 0$ and the structural parameters shown in Tab. 2.

$$I(\ddot{\theta} + 2\zeta\omega_n\dot{\theta} + \omega_n^2(\theta - \theta_i)) = M_\theta \tag{16}$$

Results of the numerical simulations are compared with the solutions of Eqn. (17), which is Eqn. (4) adapted with our model and assumptions:

$$\ddot{\theta} + \omega_n \frac{U_R}{2\pi I^*}\left(A + B\frac{\partial C_\theta}{\partial \theta}(\theta)\right)\dot{\theta} + \omega_n^2\left(\theta - \theta_i - \frac{U_R^2}{8\pi^2 I^*}C_\theta(\theta)\right) = 0 \tag{17}$$

Tables 3 and 4 show the critical reduced velocity and limit cycle amplitudes for several values of initial angle. Comparison is made between our non-linear model and the full numerical simulations.

The critical reduced velocity is measured from the period of the free oscillations simulations. The angle of equilibrium is taken as the middle between the top and bottom extrema of the signal, when a limit cycle is reached, or the final angle when oscillations are totally damped. The amplitude Θ is measured on the limit cycle. These criteria show the consistency between the non-linear model and the numerical experiments.

Table 2: Structural parameters for free motion cases.

Geometry	m^*	k_s	I^*
Square	100	0.411	16.67
Bundle	100	0.123	4.99
Rectangle $R = 4$	3662	2.00	81.06
Rectangle $R = 10$	9630	2.00	81.06

Table 3: Results analysis, square

AOA	FSI			Model			Blevins
θ_i	U_r	θ_e	Θ	U_r	θ_e	Θ	criterion
0	36.3	0	27	36.1	0	24	Yes
5	36	3	20	36.1	4.3	23	Yes
10	35.4	6.5	16	36.4	8.5	22	Yes
15	37.9	10	No	37.9	9.8	No	No
20	43.3	15	No	42.7	14.9	No	No

5 Modelling with a 2nd order Taylor expansion

We see that prediction of the free motion is good for the two sections we first studied. We assess the validity of the model with new geometries, rectangles with aspect ratios of 4 and 10. The typical size of the cylinder is its length $D = 1$ and we characterize the geometry with the aspect ratio $R = D/l$, where l is the width of the cylinder. The convention is $\theta = 0$ when the section is horizontal. Moreover, we change the forced-motion law from the sinus to a triangle, to set angular acceleration to zero on most of the motion. But our two-coefficients model has very poor results with rectangles, so that we expand the added damping to the 2^{nd} order in position and velocity, around the average angle θ_e, to build a more generic model:

Table 4: Results analysis, bundle

AOA	FSI			Model			Blevins
θ_i	U_r	θ_e	Θ	U_r	θ_e	Θ	criterion
-15	35.3	-12	No	35.6	-11.8	No	No
-10	34.5	-8	2	34.7	-8.3	10	Yes
-5	35.7	-4	19	34.5	-5.0	17	Yes
0	35.7	-1.4	21	34.4	-1.3	19	Yes
5	35.4	2	20	34.6	2.5	19	Yes
10	35.7	5	17	34.7	6.1	16	Yes
15	34.5	9	5	34.3	9.1	4	Yes
20	37	13	No	36.3	12.9	No	No

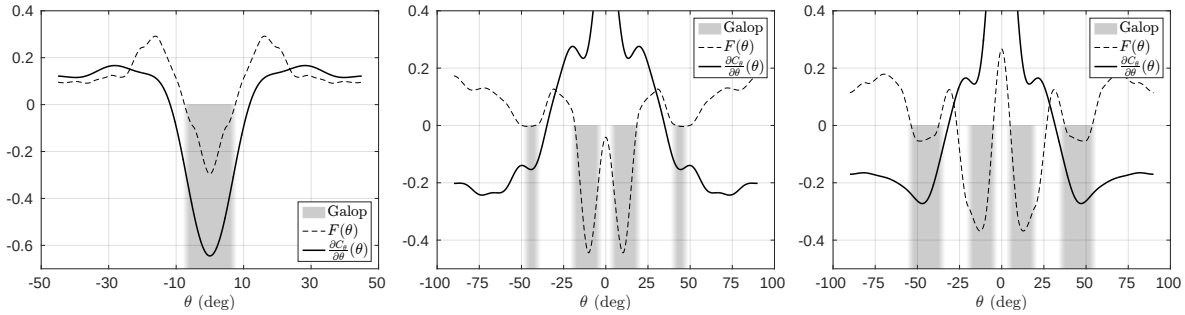

(a) Square (b) Rectangle, $R = 4$ (c) Rectangle, $R = 10$

Figure 8: Added damping, Blevins criterion and galloping zones, for square and rectangular sections.

$$C_{D\theta}(\theta, \dot{\theta}) = a + b(\theta - \theta_e) + c(\theta - \theta_e)^2 + d\left(\frac{\dot{\theta}}{\omega_n}\right) + e\left(\frac{\dot{\theta}}{\omega_n}\right)^2 + f\left(\frac{(\theta - \theta_e)\dot{\theta}}{\omega_n}\right) \tag{18}$$

The six coefficients can be obtained from our numerical experimental data. Our first model suggests that the effect of the angular velocity on the damping can be neglected. We noticed in this second model that d, e and f are not equal to zero, but their value is small compared to other coefficients, so that we came to the same conclusion: $C_{D\theta}(\theta, \dot{\theta}) \simeq F(\theta)$. A least square minimization gives the function F. To investigate if Blevins criterion makes sense with the new streamlined geometries, we plot on Fig. 8 the damping as a function of the position ($F(\theta)$), the derivative of the static moment coefficient and the unstable zones. It appears clearly that our measure of the damping is accurate, as a negative damping corresponds to the galloping positions. But we notice that a negative slope of the moment coefficient is not always linked to a negative damping: Blevins criterion is wrong for rectangular geometries. The success of the first model is only a consequence of the similarity between the damping and the derivative of the moment coefficient for the square section. To determine the unstable zones, the free motion simulations have been done with the parameters in Tab. 1 and no structural damping. Note that the average position of the cylinder strongly depends on the reduced mass through the structural stiffness, for a given reduced velocity. We selected high reduced masses to limit the static deflection of cylinders, but it made the time to reach the limit cycle too long. Nevertheless, the prediction of the unstable angles of equilibrium from the Taylor expansion approach works far better than models obtained with Blevins assumption.

Nomenclature

Solid parameters

D	Typical size of the cylinder section
ρ_s	Solid dendity
M_θ	Fluid moment on the cylinder section, around the structural central axis
c_s	Structural damping
k_s	Structural stiffness
I	Inertia per unit length of the section
θ_i	Initial angle, for which the torsion spring does not exert any torque
θ_e	Equilibrium angle under fluid moment
Θ	Amplitude of the forced motion

Fluid parameters

U	Fluid transverse velocity
ρ_f	Fluid density
μ_f	Fluid dynamic viscosity

Non dimensional parameters

$Re = \rho_f U D/\mu_f$	Reynolds number
R	Aspect ratio of the section
$t_f = Ut/D$	Fluid time
$t_s = \omega_n t$	Solid time
$U_R = 2\pi t_f/t_s$	Reduced fluid velocity
$m^* = \rho_s/\rho_f$	Reduced mass
$\zeta = c_s/2\sqrt{k_s I}$	Structural damping ratio
$I^* = I/\rho_f D^4$	Inertia number
C_θ	Coefficient of moment
K_θ	Flow induced stiffness
$C_{D\theta}$	Fluid added damping
I_θ	Fluid added inertia

References

[1] D. Pelletier A. Joly, S. Etienne. Galloping of square cylinders in cross-flow at low reynolds numbers. *Journal of Fluids and Structures*, 28:232–243, 2012.

[2] R. Blevins. *Flow-Induced Vibrations*. Van Nostrand Reynolds, New-York, 2^{nd} edition, 1990.

[3] AR Bokaian and F Geoola. Hydroelastic instabilities of square cylinders. *Journal of Sound and Vibration*, 92(1):117–141, 1984.

[4] Stéphane Étienne, André Garon, and Dominique Pelletier. Perspective on the geometric conservation law and finite element methods for ale simulations of incompressible flow. *Journal of Computational Physics*, 228(7):2313–2333, 2009.

[5] Michael P Païdoussis, Stuart J Price, and Emmanuel De Langre. *Fluid-structure interactions: Cross-flow-induced instabilities*. Cambridge University Press, 2010.

[6] I Robertson, L Li, SJ Sherwin, and PW Bearman. A numerical study of rotational and transverse galloping rectangular bodies. *Journal of Fluids and Structures*, 17(5):681–699, 2003.

[7] Dong-Hyeog Yoon, Kyung-Soo Yang, and Choon-Bum Choi. Three-dimensional wake structures and aerodynamic coefficients for flow past an inclined square cylinder. *Journal of Wind Engineering and Industrial Aerodynamics*, 101:34–42, 2012.